



Measurement of additively manufactured freeform artefacts: The influence of surface texture on measurements carried out with optical techniques

Maria Grazia Guerra^{a,*}, Fulvio Lavecchia^a

^a Department of Mechanics, Mathematics and Management, Politecnico di Bari, Via Orabona 4, 70125 Bari, Italy

ARTICLE INFO

Keywords:

Metrology for additive manufacturing
Surface texture
Optical measuring techniques
Metrological filters
High resolution mesh
Freeform artefact

ABSTRACT

Quality control of additively manufactured parts is a crucial topic, since it includes the measurement of freeform geometries, i.e. lattice structures, and parts characterized by surface topographies several times more rough than conventional machining. Freeform surfaces and their related measurands can be effectively assessed via areal optical scanning techniques and X-ray-based systems, while it is still of great interest to evaluate the effect of the surface quality on their measuring performance.

In this work, an experimental investigation about the influence of a typical additive manufacturing surface texture on optical measurements was conducted. As test object, the geometry of a standard freeform artefact developed by the NPL Institute was considered and it was realized by using a Material Extrusion Additive Manufacturing (MEX) technology and micro-milling. By comparing results coming from the two realized artefacts, it was possible to evaluate the influence of the AM surface texture on the conducted measurements.

1. Introduction

The measurement of additively manufactured parts is currently a topic of great discussion, although there is still a gap concerning the geometric specification and metrology. Additive Manufacturing (AM) opened the possibility to realize complex structures not feasible with other manufacturing techniques, posing a crucial challenge for most of the already existing measuring instruments [1].

Some of the main challenges that AM brought in the field of coordinate metrology are related to complex freeform shapes, re-entrant features, occlusions and surface texture with typically high roughness. Moreover, AM technologies involves the use of a wide range of materials, polymers, metals, composites characterized by different properties. As a consequence, measurement errors may arise, leading to different results according to the measuring principle adopted [1,2].

The measurement of freeform shaped objects is a topic already discussed in literature [3,4].

If just the geometrical complexity is considered, a non-contact measuring system could be selected as the best choice thanks to its capability to acquire large amounts of points in short time, regardless the complexity of the object's shape. Although, there are still issues related to the traceability of those systems, which strongly depends on the considered measuring task. Generally, from a metrological point of

view, Coordinate Measuring Machines (CMMs) are still considered the best choice for dimensional verifications with low uncertainties. Although, their traceability is not completely assured when measuring freeform objects [3] and sampling strategies are crucial for determining the accuracy and the efficiency of the measuring process [5–7]. Optical 3D scanning techniques and X-ray Computed Tomography (XCT) are usually adopted for the measurement of freeform artefacts and their performances have been analyzed considering different configurations and conditions [8–12]. When a freeform shaped part is fabricated by AM technologies, the measuring task is further complicated due to the peculiar surface topography generated by the process, several times more rough than conventional machining.

Tactile CMMs are not ideal for providing a reference measurement of AM parts since they acquire a mechanically filtered surface [13] and they are not able to catch small-detailed features [14], while non-contact measurement techniques are able to acquire more surface details according to their resolution capabilities [14–16]. The surface texture characterizing AM parts is known to affect the uncertainty of measurements conducted with different measuring instruments, both contact and non-contact, with systematic and random effects, which need to be better understood and quantified [17].

Few works have been conducted on the influence of different surface topographies on non-contact measuring methods: in [18] the offset

* Corresponding author.

E-mail address: mariagrazia.guerra@poliba.it (M. Grazia Guerra).

between measurements conducted with a CMM and three non-contact measuring instruments caused by surface roughness was investigated and a significant correlation trend was detected. In [19] the influence of surface roughness generated by a metal AM process was evaluated and comparisons were made with respect to CMM measurements. In [20] the surface roughness influence on turned cylinders measured by XCT was evaluated. While in [21], an experimental study was conducted to evaluate the influence of the surface roughness on XCT measurements by using workpieces produced by AM and calibrated by tactile CMM. Systematic biases comparable with the roughness values were found to affect measurements.

Among optical 3D scanning systems, laser-based, structured light and photogrammetry-based scanners are mainly used [4,8,10–12,22,23]. In [10] a structured light scanner and a photogrammetry-based scanner were used for measuring complex freeform additively manufactured parts and their performances were evaluated considering a novel set of indicators describing surface coverage, sampling density and measuring errors. In [22], measurements of an additively manufactured test artefact realized by High Speed Sintering (HSS) were conducted with CMM, XCT and photogrammetry. Results from [10] and [22] confirmed the complexity of evaluating AM parts mainly due to the surface roughness which, for certain high values, can lead to highly different results according to the measuring principle adopted. This makes as well difficult to compare different measuring instruments and to state which is the most accurate and reliable for a specific measuring task, since the reference measurement is not clearly determined.

Recently, the possibility to evaluate surface texture parameters from highly detailed meshes emerged [24,25] and it opened the possibility to use non-contact measuring techniques, usually implemented for dimensional and geometrical metrology, for surface quality assessment, as long as the resolution is sufficient [26].

First of all, a form needs to be associated with the freeform surface (called “shell”). Thus, surface quality parameters are computed as deviations associated with each point of the freeform surface. When a general surface cannot be fitted with a primitive geometrical form, the application of filtration algorithms becomes necessary to compute a smooth version of the shell, which can be considered as a waviness surface. Deviations are then calculated between the original freeform surface and the smoothed shells obtained after the filtering process. This latter can be achieved by using several filtration algorithms: a pseudo-Gaussian filter, a Bilatéral filter and a mean curvature flow filter [27]. It is then possible to decompose the highly detailed mesh and separate shortwave and longwave components according to different *cut-off* values.

As high-resolution 3D scanning methodology allow, potentially, the extraction of surface texture parameters, they are also significantly affected by the same surface texture when used for dimensional and geometrical metrology.

The aim of the present paper is to conduct an experimental investigation on the influence of a typical AM surface texture on measurements conducted with optical methods characterized by different measuring principles and resolutions. With this aim, three measuring instruments were considered: a photogrammetry-based system, a conoscopic holography laser scanner and a structured light scanner, usually adopted for dimensional and geometrical metrology. The analysis was carried out considering a free-form artefact, whose geometry is a down-scaled customization of the standard artefact developed by the NPL Institute [28]. The artefact was realized by using Material Extrusion Additive Manufacturing (MEX) and, in order to have a reference for the measurement analysis, it was also realized by micro-milling. The influence of surface texture on the three considered measuring instruments was analyzed by means of 3D comparisons, 2D sectional comparisons and feature analysis. Metrological filters recently implemented for the surface texture assessment starting from freeform meshes [2527] were also applied to eliminate the short wavelengths and results were then re-

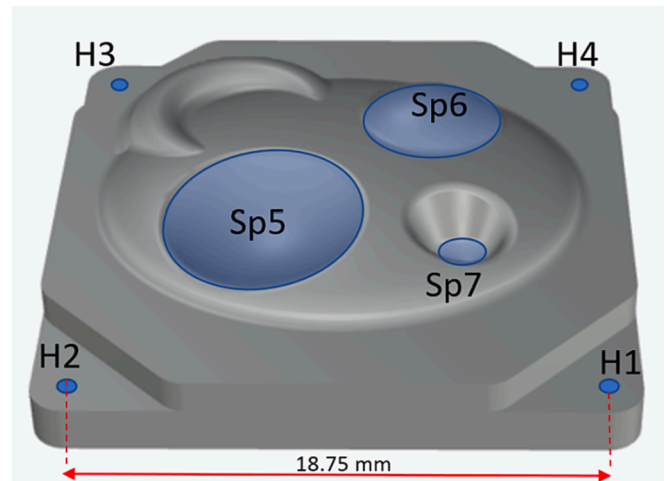


Fig. 1. NPL CAD model and main feature.

Table 1

CAD dimensions of the NPL artefact adaptation with 18.75 mm of characteristic distance.

Feature ID	Nominal value [mm]
H1-H2	18.75
H2-H3	18.75
H3-H4	18.75
H4-H1	18.75
Sp5	10.622
Sp6	8.124
Sp7	2.499
Sp5-Sp6_distance	11.197

examined and discussed.

2. Materials and methods

2.1. Customized NPL artefact

Measuring a test artefact is one of the most used approaches for evaluating the performance of measuring systems [29] and in this work, a customized freeform artefact, which is the down-scaled version of the original artefact developed by the NPL Institute (150x150x40 mm³) was considered as test measuring object [28]. The artefact features both concave and convex shapes and it was originally realized with highly reflective material, 6082-T6 – Aluminium Dural, with the aim to identify the weaknesses of optical-based system. In this work it was scaled with a scale factor of 1:8 in order to cover the measuring volume suitable for the reconstruction of sub-millimeters features. This way it was possible to test optical scanners characterized by different resolutions and working volumes. The modified version of the NPL artefact is reported in Fig. 1. The main artefact dimensions are reported in Table 1.

The custom NPL artefact was then realized by MEX using a Zortrax M200 and a proprietary material, grey Acrylonitrile butadiene styrene (ABS), supplied as a spool of filament with 1.75 mm of diameter. The same material (ABS) of the same color (grey) showed a low translucency and the minimum subsurface scattering effect in a previous study [2]. The nozzle diameter was 0.4 mm and the layer thickness was kept to its minimum value and it was set to 0.09 mm. The building orientation is shown in Fig. 2 and the artefact was XZ oriented, meaning that the freeform surface and its main feature were characterized by the layer-wise surface texture. From now on, this artefact will be re-called as FFF-NPL.

The micro-milled NPL, Fig. 3-a, was manufactured using a 5 AXIS CNC machine Kugler MicroGantry® micro3/5X Laser with 60,000 rpm

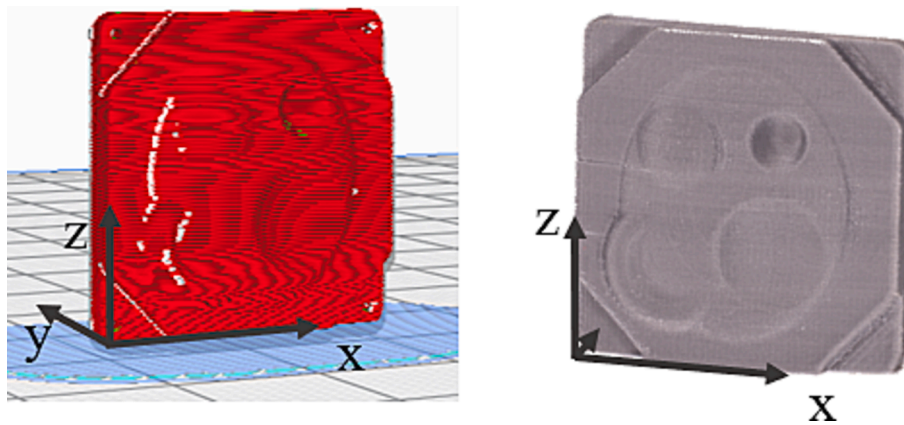


Fig. 2. FFF-NPL with indication of the building direction.

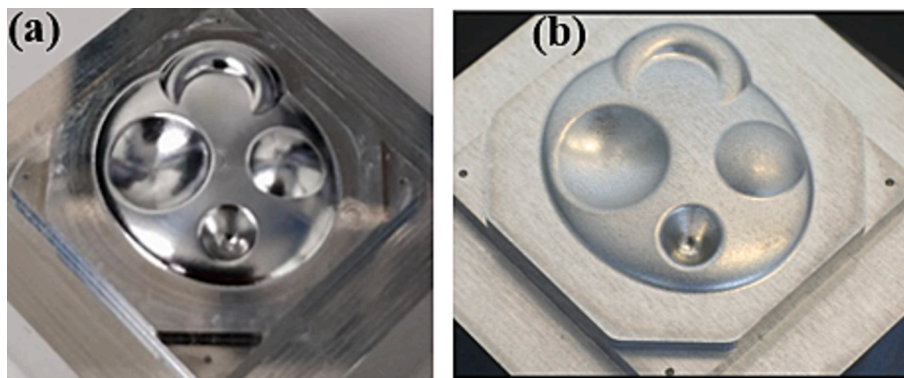


Fig. 3. Micro-milled NPL (a) micro-milled NPL after chemical etching (b).

of maximum spindle speed and a positioning accuracy of $\pm 1 \mu\text{m}$ along the x axis and $0.5 \mu\text{m}$ along y and z axes. The machining was conducted using three out of five axes and using a ball milling tool for the finishing process with 1 mm of diameter and 0.5 mm of edge radius. The artefact was realized with 6082-T6 Aluminum Dural, same material of the standard artefact shown in [28]. It was subsequently etched with acid in order to reduce the surface reflectance, see Fig. 3-b. From now on, this artefact will be re-called as Al-NPL.

Surface texture of each realized artefact was measured by using an optical profiler CCI-MP-HS Taylor Hobson based on interferometry equipped with a 20x lens with a xy resolution of $0.1 \mu\text{m}$ and declared z resolution of 0.1 \AA .

Profile roughness parameters were computed according to the ISO 21920-2:2021. The micro-milled NPL showed an R_a of $0.003 \mu\text{m}$ and an R_z of $0.014 \mu\text{m}$ using a L-filter nesting index N_{ic} (cut-off λ_c) of 0.25 mm, while the FFF-NPL was characterized by R_z equal to $40.4 \mu\text{m}$ and an R_a of $5.97 \mu\text{m}$ and in this case the L-filter nesting index N_{ic} was set to 2.5 mm. Due to the building direction, the FFF-NPL showed also a main texture direction of approximately 89.9° .

2.2. Optical measuring instruments and methods

The artefacts shown in Section 2.1 were acquired by different optical measuring instruments with different working principles and resolutions and they are listed as follows:

- a laser-based sensor exploiting the conoscopic holography (CH) principle, Optimet Conoscan 3000, with a 50 mm lens and an optical resolution of 0.01 mm.

- a Photogrammetric Scanning System with Rotary Table (PSSRT) already implemented and used for measurement in close and micro range [2,12,30]. It is a motorized and controlled scanning system with a great flexibility and working volumes ranging from a very small volume $18 \times 18 \times 10 \text{ mm}^3$ to bigger ones, like approximately $150 \times 150 \times 40 \text{ mm}^3$. The working volume strictly depends on the chosen optical configuration and, consequently, the resolution of the system varies. In this work a Canon Eos 760D with a Canon EF 50 mm 1:1.8 II lens with an extension tube of 36 mm was used and a ground resolution of 0.009 mm/pixel was achieved. Camera was tilted at 45° allowing the reconstruction of both concave and convex features. The rotary stage chosen was 5° and, consequently, 72 was the number of acquired images. The image processing step was conducted with Agisoft Metashape. The scale factor was computed through the distance between coded targets placed around the object.
- a commercial Structured Light Scanner (SLS), ATOS Q 8 M supplied by ZEISS GOM Metrology, with a working area of $100 \times 70 \text{ mm}^2$ and a declared resolution of 0.04 mm (from manufacturer specification).

A tactile CMM, DeMeet 400 (MPE X/Y/Z = $3.97 \mu\text{m}$), with a ruby touch probe of 2 mm of diameter, was also used for the feature measurements.

All measurements were carried out in a temperature-controlled environment at $20 \pm 0.5^\circ \text{C}$. The analysis of the scanners outputs was conducted with the GOM inspect software for both 3D and 2D section comparisons and for the feature analysis.

The Least Square Method (LSM) was used for the features fitting. Both bidirectional (sphere diameters) and unidirectional (distances between spheres) lengths were investigated. When measuring additively

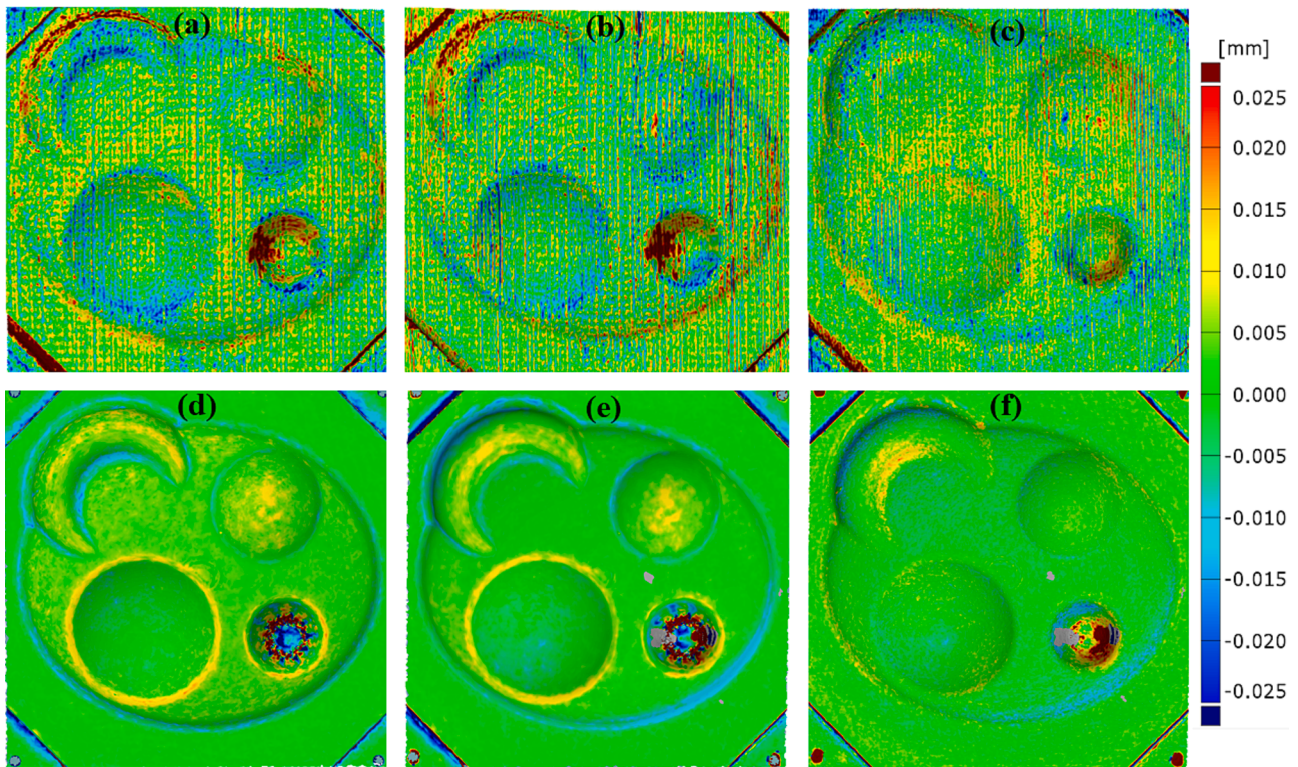


Fig. 4. 3D comparisons between 3D models of FFF-NPL in (a) PSSRT-SLS, (b) CH-SLS, (c) PSSRT-CH and of the AI-NPL in (d) PSSRT-SLS, (e) CH-SLS and (f) PSSRT-CH.

manufactured parts, the peculiar texture and the staircase effect highly affect the uncertainty of measurement. Thus, some parameters describing the quality of the fitting process were considered, such as the *residual* and the maximum absolute deviation (*max dev*) describing how the ideal geometry fitted the used points [31]. The first is defined as the absolute average distance computed between each point of the measured surface and the corresponding one on the fitted geometry. The *max dev* is defined as the maximum absolute deviation registered between the considered points and the fitted geometry.

3. Results and discussion

3.1. Initial data analysis

At first, 3D models of the FFF-NPL and the AI-NPL obtained with CH, PSSRT and SLS were compared, in pairs, and colored maps of deviations are reported for the FFF-NPL in Fig. 4-a, Fig. 4-b, Fig. 4-c and for the AI-NPL in Fig. 4-d, Fig. 4-e, Fig. 4-f.

As a general comment, differences between measuring instruments appeared more pronounced when considering the FFF-NPL artefact with respect to the AI-NPL with deviations mostly comprised within ± 0.01 mm, while the artefact fabricated by micro-milling registered deviations mostly comprised within ± 0.005 mm (Sp7 was still critical to measure with the CH and SLS and it was the reason for the high deviations registered in that area). Keeping fixed the artefact and considering each pair of compared instruments, higher deviations were registered when instruments with different resolutions are compared. Thus, differences between PSSRT and SLS and between CH and SLS were higher than the ones registered between PSSRT and CH, characterized by similar resolutions. It is worth noting how for the FFF-NPL, deviations are mostly distributed as vertical stripes retracing the staircase effect due to the MEX fabrication process.

A 2D section analysis was also conducted considering a XZ section extracted on the planar surface, see Fig. 5-a. Diagrams of deviations

associated with the FFF-NPL and the AI-NPL are then reported in Fig. 5-b and Fig. 5-c, respectively, considering the comparisons of measuring instruments, in pairs. On the y axis the deviation value in mm is reported, while on the x axis the section length in mm. This representation allowed to easily compare the observed deviations with respect to the primary profile evaluated on the considered surface. As it is possible to observe, values are mostly comprised between ± 0.010 mm and ± 0.015 mm for the FFF-NPL, which is a range comparable with the primary profile evaluated with the optical profilometer. The same evaluation was conducted considering the comparison between measuring instruments on the AI-NPL. In this case, diagrams of deviations showed a range comprised between ± 0.005 mm for all pairs of measuring instruments involved, showing good agreement between the optical measurements. Moreover, this range of deviations is on the same order of magnitude of the measuring accuracy of the involved instruments. Thus, if the AI-NPL is considered as reference artefact, thanks to its high manufacturing accuracy, sub-micrometer surface roughness and its non-reflective surface, the higher deviations between measuring instruments registered for FFF-NPL are mainly attributable to the surface texture influence.

To enhance this concept, a more detailed feature analysis was conducted for each artefact and each measuring instrument involved. Both bidirectional (sphere diameters) and unidirectional (distances between spheres) lengths were investigated, and measurements evaluated on the AI-NPL and on the FFF-NPL are reported in Fig. 6. Each measurement result was the average of 5 repetitions. Standard deviations coming from five repetitions are reported as error bars. As it is possible to observe, feature diameters and distances measured with different instruments were quite similar and comprised in a range (MAX-MIN) of 0.004 mm for the Sph5, 0.003 mm for the Sph6 and 0.005 mm for the Sph5-Sph6 distance. Comparing the obtained results from the optical measuring instruments with the CMM, registered deviations were approximately on the order of 0.005 mm. The Sph7 was not included in the analysis due to the high reflections observed while using the SLS and the CH.

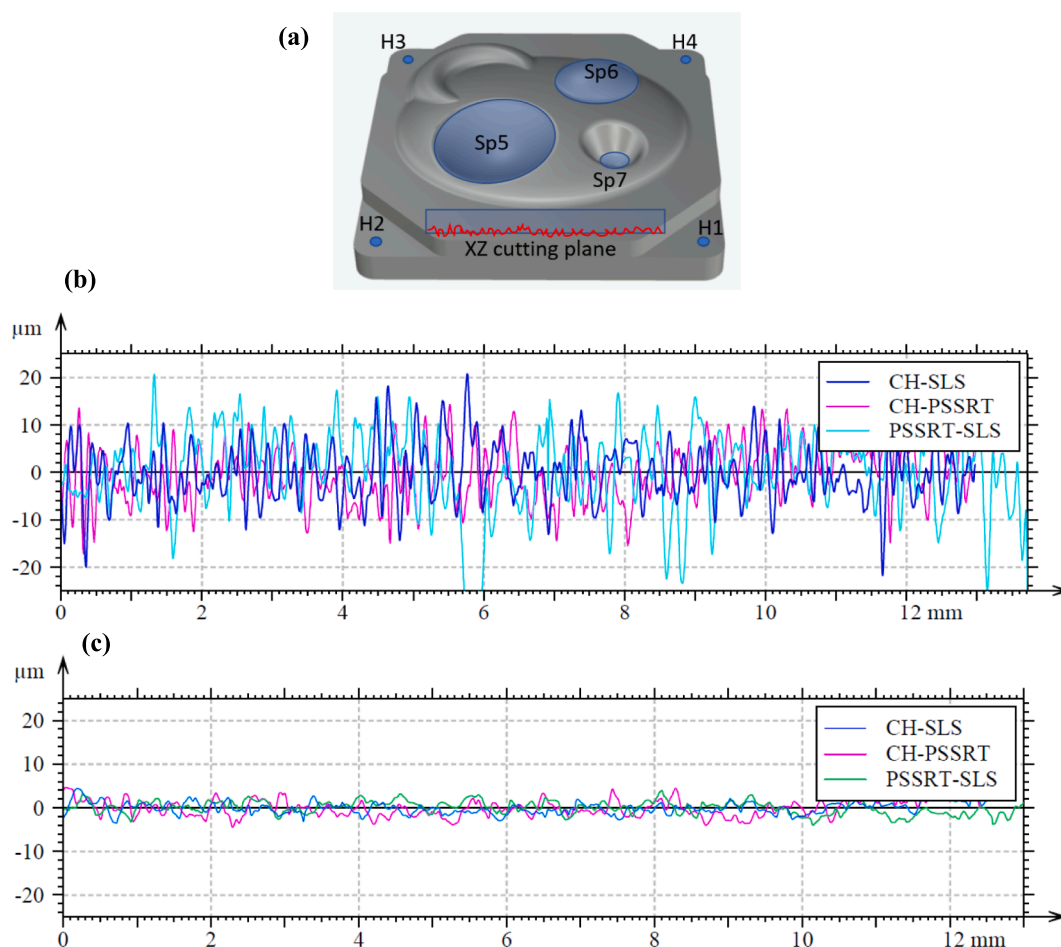


Fig. 5. 2D section analysis deviations diagrams evaluated along the XZ section (a). In (b) data retrieved on the FFF-NPL and in (c) data retrieved on the AI-NPL.

When considering the FFF-NPL, results coming from different measuring instruments varied within a wider range: 0.09 mm for the Sph5, 0.05 mm the range for Sph6 and 0.06 mm the range for Sph5-Sph6 distance, showing that different resolutions led to different measuring results when dealing with highly rough surfaces. Comparing the obtained results with the tactile CMM, the registered deviations were higher than the ones registered for the AI-NPL. In this case, considering a bias between CMM and optical methods comparable to the bias between CMM and XCT found in [21], the values of the diameters corrected for that bias (CMM \pm Rz/2) was more similar to the SLS measured value.

Apart from the mere dimensional assessment and comparison, other significant outputs, likely affected by the surface texture, were considered: the *residual* and *max deviation*.

These parameters were computed for each feature and each measuring instrument involved. Results are reported in Fig. 7 as average values of the measurements carried out on the Sph5 and Sph6.

As it is possible to observe from Fig. 7, the *residual* was below 0.005 mm for the AI-NPL, while it was higher than 0.01 mm for the artefact realized by MEX. The max deviation was on the order of 0.01 mm for the AI-NPL and on the order of 0.045 mm for the FFF-NPL.

Results from the 3D and 2D comparisons and from feature analysis showed an increase of the differences between the three investigated optical measuring methods, in terms of dimensional deviations and of the feature fitting quality, when increasing the surface roughness.

3.2. Application of metrological filters to highly detailed meshes

In order to corroborate the obtained results, the high-resolution 3D models obtained with CH and PSSRT were low-pass filtered by using

proper Gaussian filters and setting different *cut-offs* (λc). As already explained in the Section 1, surface analysis softwares recently added to their functionalities the possibility to evaluate the surface topography of free-form shaped parts by using high-resolution meshes obtained from non-contact measuring instruments [24,25]. Being this novel feature able to extract the surface topography, surface filtering algorithms are necessary in order to separate the waviness surface characterized by long wave components from the short wavelengths. Surface texture parameters can be then calculated as deviations between the original freeform surface and the smoothed shells obtained after the filtering process [27]. In this case, metrological filters were not used for surface topography evaluation, and they were applied to the high-resolution 3D meshes in order to remove the small-scaled components, short wavelengths, according to different low-pass filtering cut-off values. The remaining shape, (characterized by long wave components) see Fig. 8, was then re-examined for each condition considering 3D models comparisons, 2D sections and feature analysis.

The minimum low-pass filtering cut-off was chosen according to the layer height of the FFF-NPL (set to 0.09 mm), while the maximum value, equal to 0.6 mm, was the maximum allowed to prevent undesired modification of the artefact shape due to its smallest detail dimension. In Fig. 9 an example of the application of a Gaussian filter (ISO 16610-21) to the primary profile of the FFF-NPL is reported with the minimum (0.09 mm) and the maximum (0.6 mm) cut-off value set.

At first, differences between the unfiltered and filtered meshes for both PSSRT and CH were evaluated in order to estimate the effect of a low-pass filter on the original and unfiltered data.

Results are reported in terms of 3D comparison and feature analysis with indication of the diameter of spheres, and XYZ coordinate of their

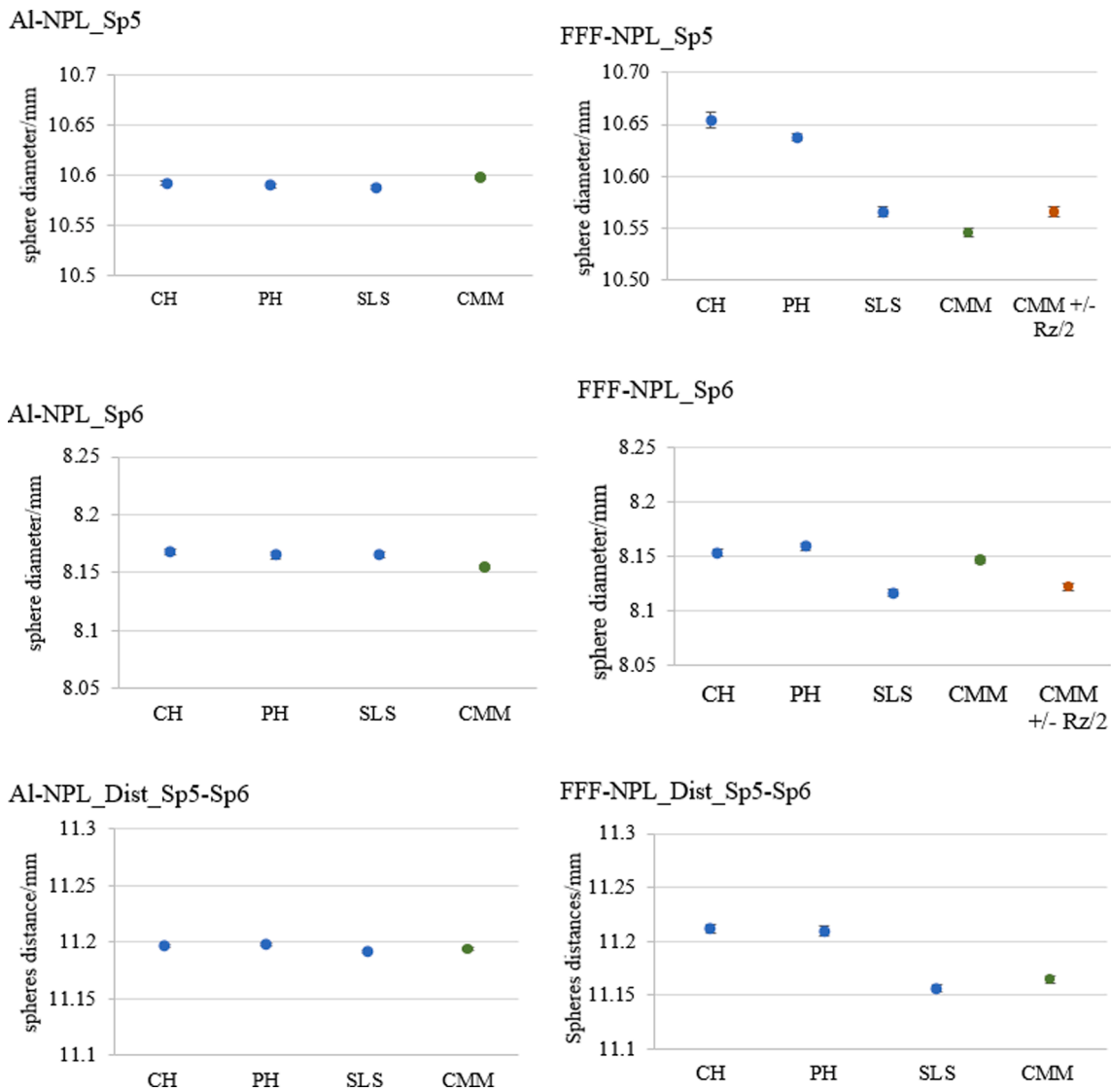


Fig. 6. Feature measurements conducted on Al-NPL and FFF-NPL.

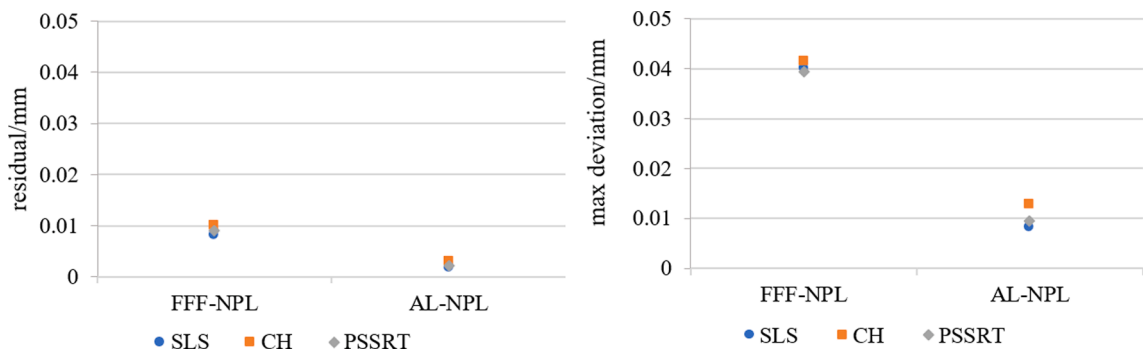


Fig. 7. Residual and maximum deviation evaluated on the Al-NPL and the FFF-NPL.

centers.

3D comparisons, shown in Fig. 10, highlighted a slight effect of the filtering when the 0.09 and 0.12 mm cut-off filters are used. This effect was more marked on the PSSRT mesh rather than the CH. It could be due to the presence of shorter wavelengths on the PSSRT meshes. Anyway, the highest differences were registered when the 0.3 and the 0.6 mm filters were applied. The most affected parts correspond to the smaller

details and connections between each feature and the elliptical surface and between the elliptical surface and the planar surface as they were characterized by a small radius. By analyzing the output of the 0.6 mm filtered mesh it is possible to observe that most of the highlighted deviations are distributed as vertical stripes corresponding to the characteristic MEX typical texture.

In order to better quantify the bias due to the filtering process, in

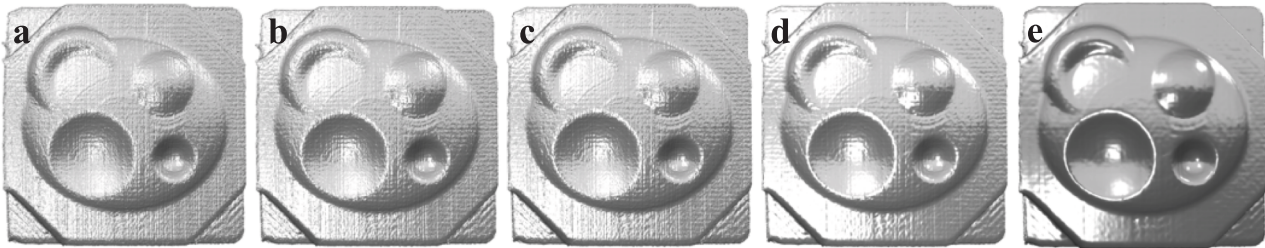


Fig. 8. Examples of filtering applied on FFF-NPL acquired by the PSSRT. (a) no filter, (b) $\lambda = 0.09$ mm, (c) $\lambda = 0.12$ mm, (d) $\lambda = 0.3$ mm, (e) $\lambda = 0.6$ mm.

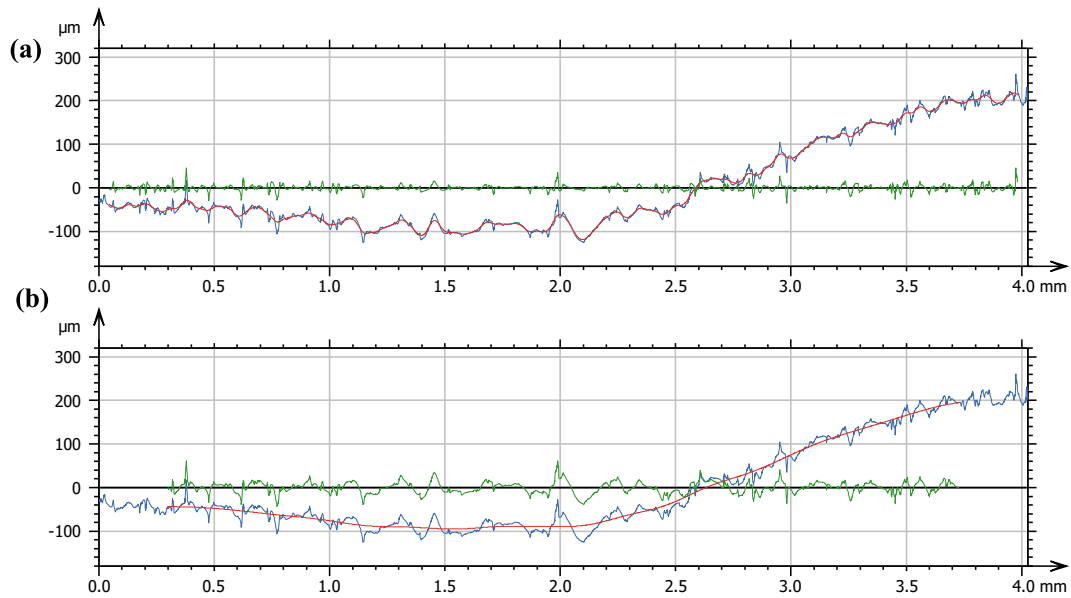


Fig. 9. Profile of the FFF-NPL filtered with cut-off 0.09 mm (a) and 0.6 mm (b). In green the roughness and in red the low-pass filtered profile (waveness). (For interpretation of the references to color in this figure legend, the reader is referred to the web version of this article.)

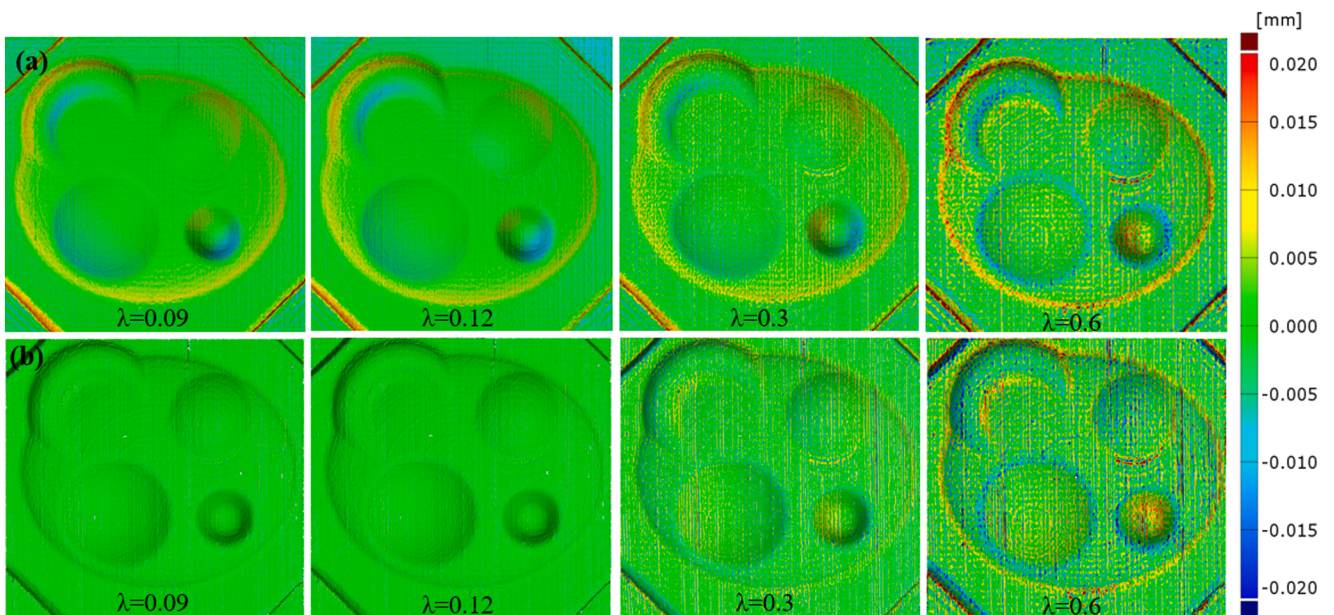


Fig. 10. 3D comparisons between unfiltered mesh and filtered meshes according to different cut-off values [mm]. In (a) the photogrammetric meshes are reported, while in (b) the mesh obtained with the CH.

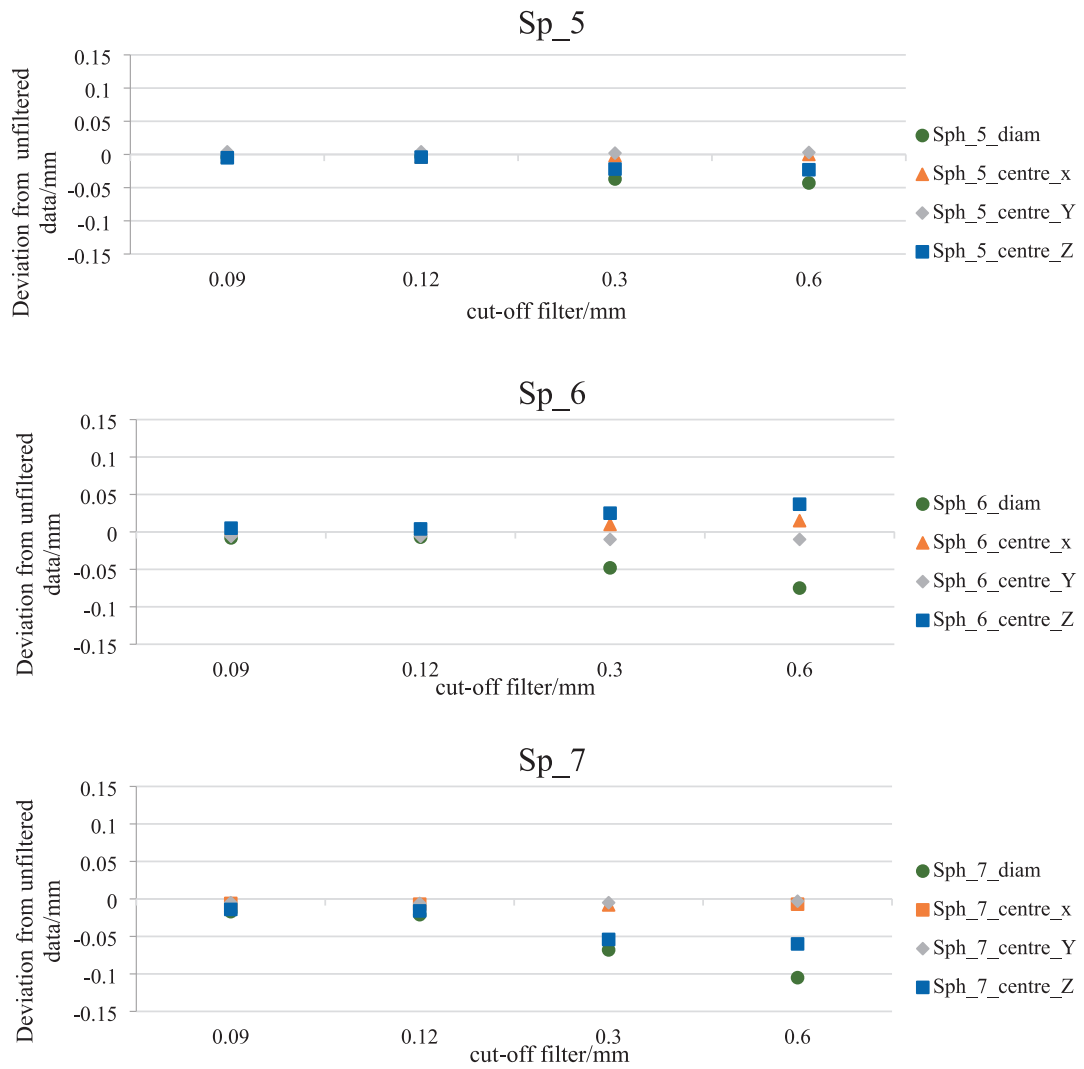


Fig. 11. Feature diameter and center coordinates deviations from the unfiltered data. This data are referred to the PSSRT case, as an example.

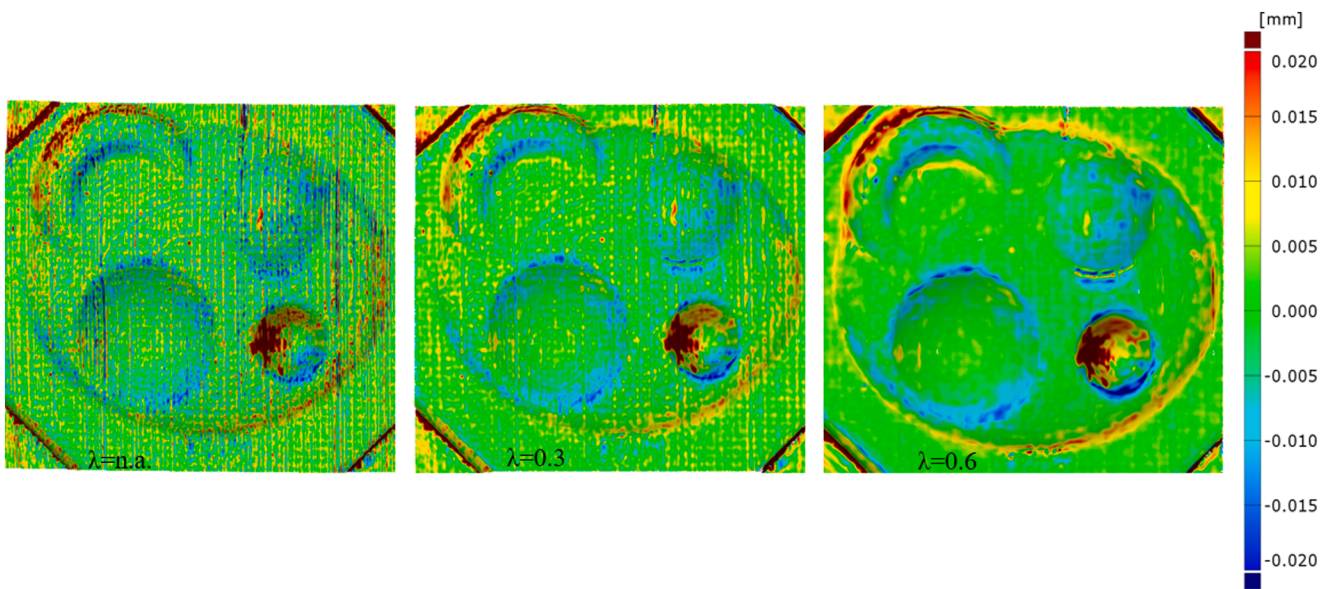


Fig. 12. 3D comparisons between the SLS and CH, considering the latter unfiltered and filtered with $\lambda = 0.3$ mm and 0.6 mm.

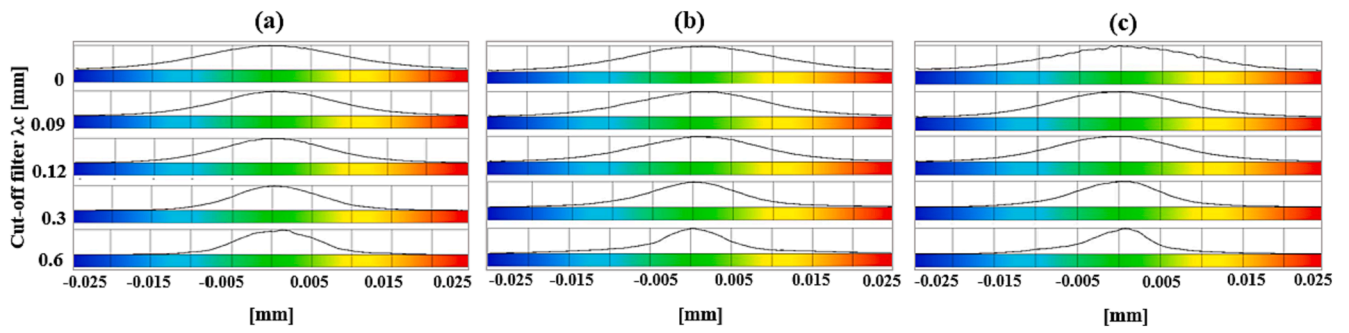


Fig. 13. Histograms of the 3D comparisons between (a) CH-PSSRT, (b) CH-SLS and (c) PSSRT-SLS for the FFF-NPL artefact. Deviations are expressed in mm.

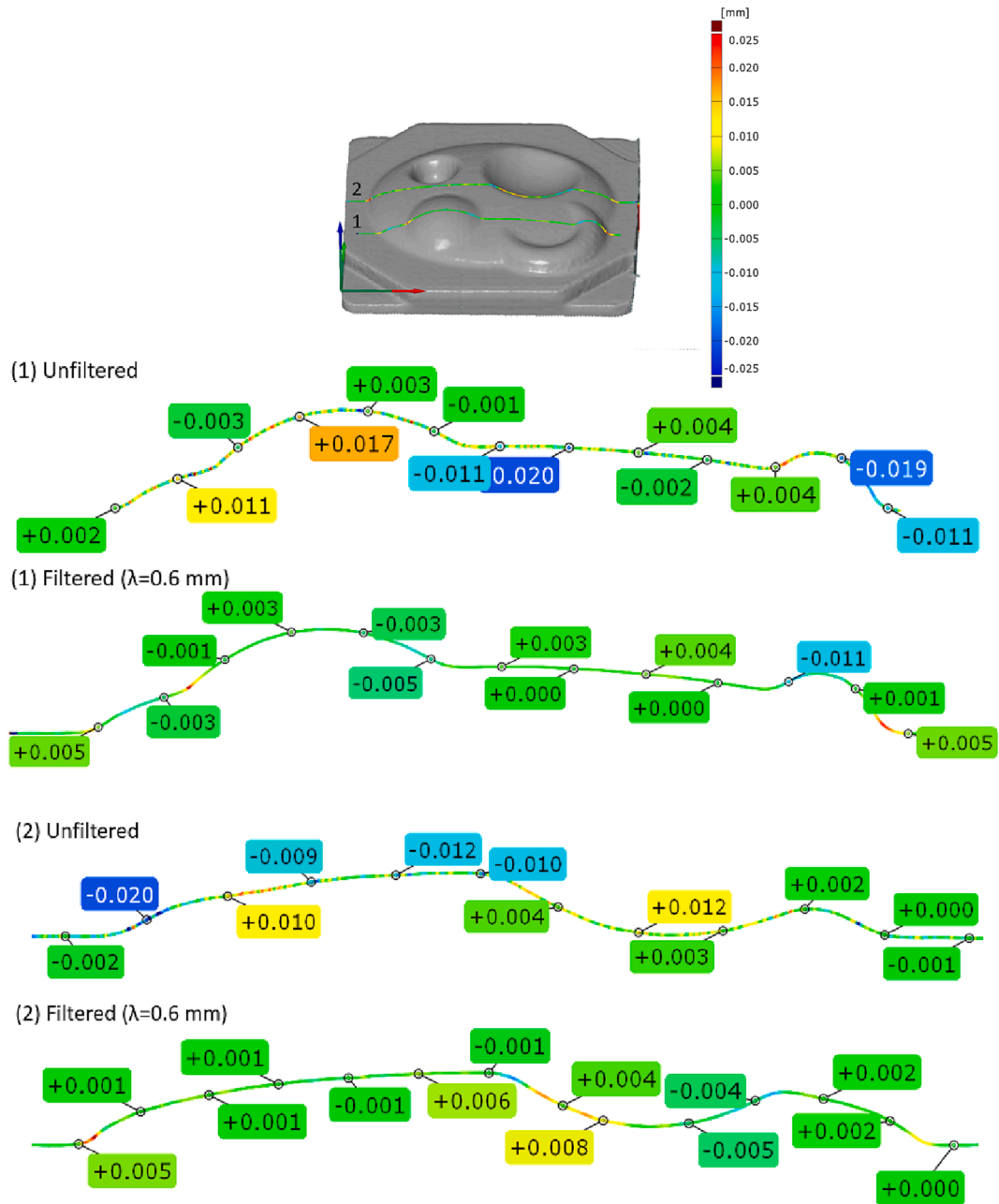


Fig. 14. 2D section analysis conducted by comparing PSSRT and SLS. Both filtered and unfiltered data are reported. Deviations are expressed in mm.

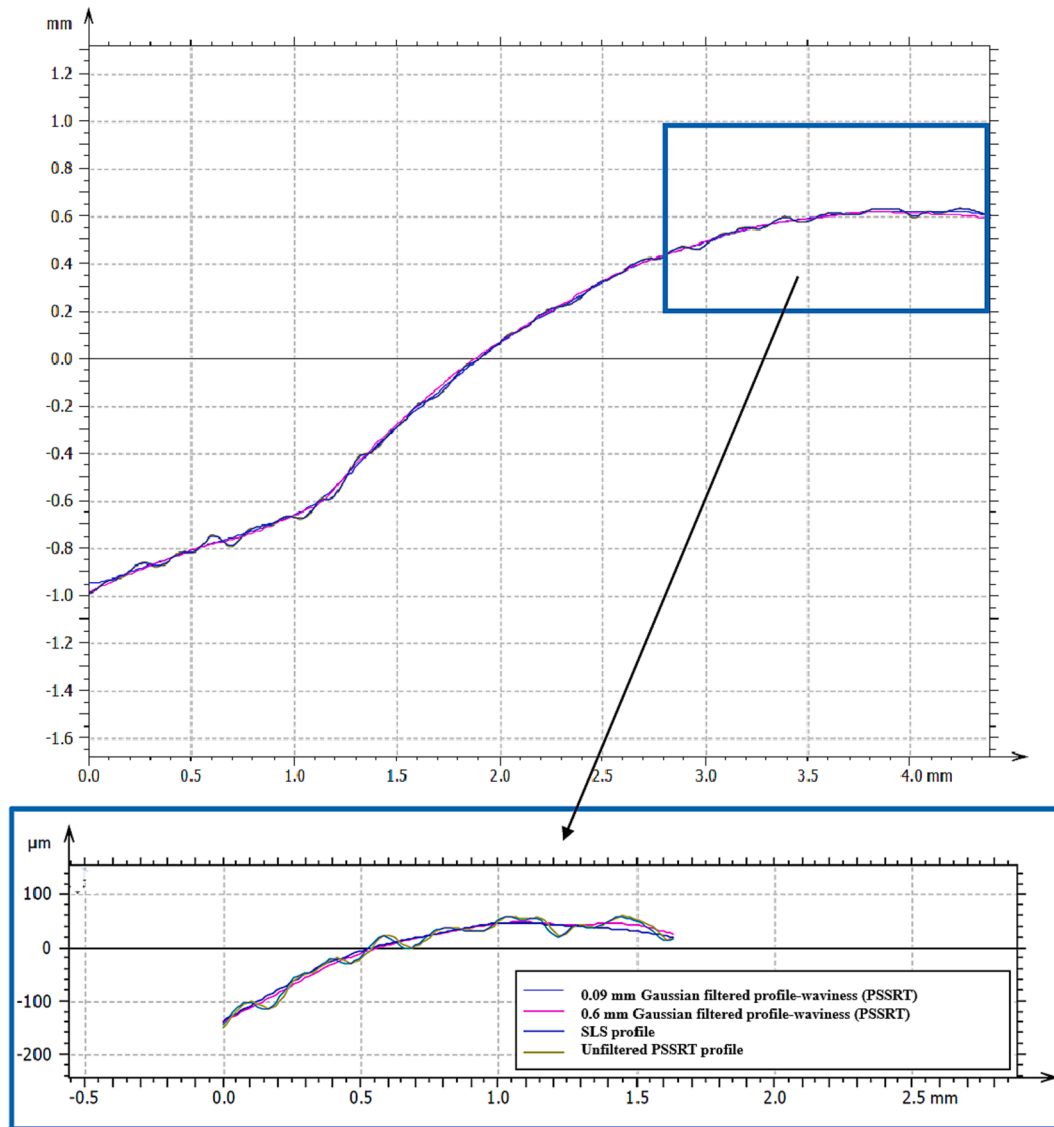


Fig. 15. Profile of the PSSRT FFF-NPL filtered with cut-off 0.09 mm and 0.6 mm and overlap with the SLS profile.

Fig. 11 the feature analysis was conducted considering the PSSRT as representative case. By analyzing each feature, it is possible to observe a general decreasing of the feature diameter and this effect was more marked for the smaller spheres, such as the Sph6 and Sph7 with values comprised between 0.05 and 0.1 mm. This difference was accompanied by a modification of the xyz center coordinates. Regarding the Sph5 the most affected coordinate was the z. Considering the Sph6 both z and y, and finally the Sph7 mostly the z. This is mainly due to the orientation of each feature.

Filtered PSSRT and CH meshes were then compared with the mesh obtained with the SLS. It is possible to observe from Fig. 12 that, by increasing the cut-off filter value, areas characterized by deviations comprised between ± 0.005 mm were more widespread. On the other hand, deviations corresponding to surface connections, characterized by small radii, remained unchanged or increased their deviations.

Histograms coming from the 3D comparisons are reported in Fig. 13 and when increasing the cut-off filtering value, the registered deviations were mostly comprised between ± 0.005 mm, getting closer to the results obtained from the AI-NPL artefact.

2D sections were also extracted from the unfiltered and filtered meshes ($\lambda = 0.6$ mm). Colored map and annotations of deviations are visible in Fig. 14. Deviations registered on the filtered meshes were

mostly comprised within ± 0.005 mm and thus comparable with deviations observed on the AI-NPL. In particular, deviations were generally lower when larger curvatures were considered, while still higher deviations were registered in correspondence of small details and surface connections.

To better understand the comparison between filtered and unfiltered data, a part of the section number 1 (Fig. 14) was taken into account, in particular the one related to the Sphere 6. Thus, the SLS profile, the unfiltered PSSRT and the filtered PSSRT (with both cut-off 0.09 mm and 0.6 mm), selected as representative case, were superimposed. As it is possible to observe on Fig. 15, differences between the unfiltered PSSRT profile and the SLS are mostly related to the AM texture pattern, while considering the filtered profile, the one characterized by 0.6 mm of cut-off showed a good overlap with the SLS profile.

Finally, the feature analysis was carried out and the dimensions evaluated on the filtered models showed more consistent values with a general reduction of differences registered among the investigated instruments PSSRT, CH and SLS. To evaluate the closeness of agreement between the conducted measurements, the standard deviation of the average values obtained with PSSRT, CH and SLS was considered, see Fig. 16.

As it is possible to observe, a reduction of the standard deviation was

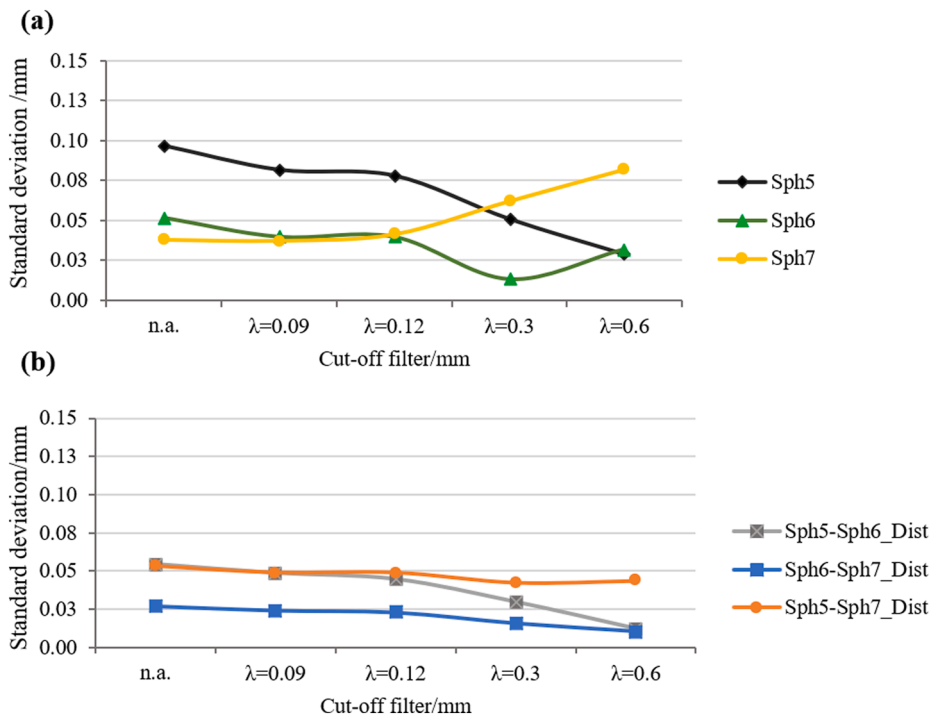


Fig. 16. Closeness of agreement between measuring instruments involved, evaluated on diameters measurements (a) and on sphere distances (b) with respect to the applied cut-off filter.

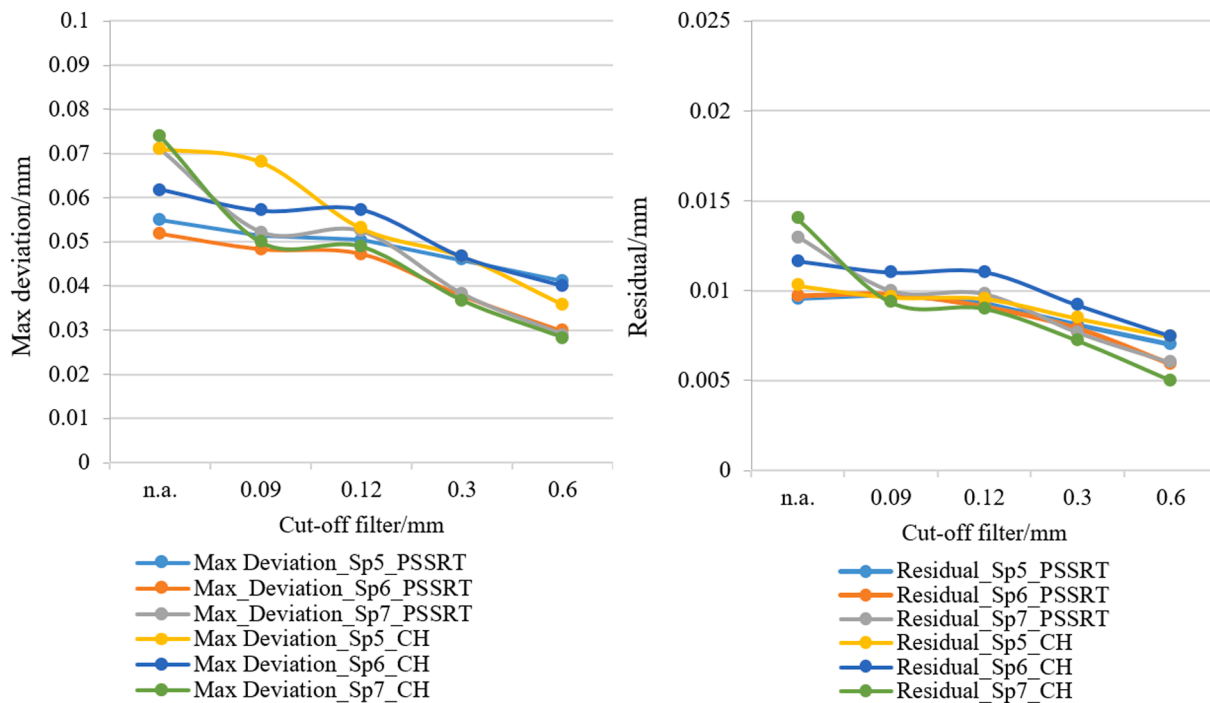


Fig. 17. Residual and Max deviation variation with respect to the filter applied.

registered for Sphere 5 and 6 when considering 0.3 and 0.6 mm of cut-off filters. Different was the behavior of the Sphere 7. In this case, differences between measured values increased as the cut-off increases. The sphere position on the artefact and its orientation makes it difficult to achieve reliable measurements. In this case, filtering the surfaces accentuated the registered deviations.

Distances between spheres remained quite stable, except for the distance between Sphere 5 and Sphere 6 for which results tended to

converge more when increasing the cut-off filter.

Considering the quality of the fitted geometry, see Fig. 17, the residual and the max deviation registered a decrease when increasing the filtering cut-off, as well. Registered values were closer to the AI-NPL values. They cannot completely converge due to higher form errors coming from the MEX manufacturing process, less accurate than micro-milling.

The application of metrological filters allowed to mitigate the effect

of the surface texture and, in some cases, to increase the closeness of agreement between the obtained measurement results getting closer to the range of deviations achieved with the micro-milled NPL, considered as reference. The proposed approach worked well when considering larger curvature and planar surfaces, while it showed some criticalities when applied for small features and mostly vertical sides.

Freeform mesh filtering is a novel feature, and it could be useful, among other things, to understand the behavior of different measuring methods characterized, as reported in this paper, by different resolutions.

It remains still difficult to choose among different measuring methods and establish which one is the most reliable and accurate when AM parts are considered and it is further complicated by the fact that measuring techniques characterized by different resolutions lead to different results. In this context, it is worth mentioning that when comparing measurements carried out with different instruments on the same physical measurand, a portion of the observed discrepancies may be due to material optical properties, in addition to surface texture.

Further works are needed for appropriately selecting the measuring instrument according to the measuring task. With this purpose, the Stedman diagram [32,33] could be a very useful tool to determine the working capabilities of the currently available measuring methods suitable for AM parts and it will be considered in future works.

4. Conclusions

In this paper, an experimental investigation on the influence of the typical AM surface texture on optical measurements was conducted. Three measuring instruments, characterized by different resolutions and working principles, were considered. The analysis was carried out on a free-form artefact, whose geometry is a customization of a calibration artefact developed by the NPL Institute. The artefact was realized by using MEX. It was also realized with Aluminum by using micro-milling with high machining accuracy and sub-micrometer roughness in order to get reference data.

From the conducted analyses, it was possible to retrieve the following key conclusions:

- When comparing the three instruments on the AI-NPL deviations were mostly comprised within ± 0.005 mm, regardless the instrument's resolution and this value is on the same order of magnitude of the estimated measuring instruments accuracy.
- The same instruments registered higher deviations when used for the FFF-NPL assessment, with deviations mostly comprised within ± 0.01 mm when considering comparable optical resolutions and ± 0.015 mm with different optical resolutions, highlighting the influence of the surface texture and its significant effect.
- A more detailed feature analysis showed quite convergent measurement results for the AI-NPL and higher differences when considering the same instruments and the FFF-NPL. Feature fitting was indeed greatly influenced by the surface texture as demonstrated by the evaluation of the *residual* and the *maximum absolute deviation*, describing the quality of the fitting process.
- From the analysis of the filtered meshes, it was possible to observe how filtering the freeform surface with an increasing cut-off decreased the differences between the measuring instruments involved, achieving more convergent results, within a range of deviations very close to the reference value obtained on the AI-NPL.

This work should be seen as a preliminary investigation on the influence of AM surface texture on optical methods characterized by different resolutions and future works will be conducted to improve the knowledge about this topic. Moreover, at least two future developments can be drawn:

- The use of metrological filters for high-resolution meshes could be a way to overcome the criticalities arising when measuring AM feature dimensions thanks to the removal of the shorter wavelengths, possibly reaching the “reference” data not always achievable with highly accurate tactile CMMs. They can be also implemented for the uncertainty assessment usually overestimated when considering optical methods and additively manufactured parts.
- The use of high-resolution optical methods for dimensional analysis as well as for surface topography evaluation of AM components starting from the same acquired data.

CRediT authorship contribution statement

Maria Grazia Guerra: Conceptualization, Methodology, Software, Data curation, Writing – original draft, Writing – review & editing.
Fulvio Lavecchia: Conceptualization, Methodology, Writing – review & editing.

Declaration of Competing Interest

The authors declare that they have no known competing financial interests or personal relationships that could have appeared to influence the work reported in this paper.

Data availability

The data that has been used is confidential.

Acknowledgements

This paper was undertaken in the context of the project # ARS01_00806 “Innovative Solutions for Quality and Sustainability of Advanced Manufacturing Processes” (grant PNR 2015–2020, di cui al D. D. del 13 luglio 2017 n. 1735) funded by Italian Ministry of Education, University and Research; the project “Sviluppo di Tecnologie connesse ai materiali e ai processi sostenibili, integrati in sistemi produttivi per il settore agroalimentare” co-funded by the University of Foggia; the Programme “Department of Excellence” Legge 232/2016 (grant no. CUP—D94I18000260001).

The author would like to thank Professor Luigi Maria Galantucci for his kind contributions to the first conceptualization of the paper.

References

- [1] R.K. Leach, D. Bourell, S. Carmignato, A. Donmez, N. Senin, W. Dewulf, Geometrical metrology for metal additive manufacturing, *CIRP Ann.* 68 (2019) 677–700, <https://doi.org/10.1016/j.cirp.2019.05.004>.
- [2] M.G. Guerra, S.S. Gregersen, J.R. Frisvad, L. De Chiffre, F. Lavecchia, L. M. Galantucci, Measurement of polymers with 3D optical scanners: evaluation of the subsurface scattering effect through five miniature step gauges, *Meas. Sci. Technol.* 31 (2020), <https://doi.org/10.1088/1361-6501/ab3edb>.
- [3] E. Savio, L. De Chiffre, R. Schmitt, Metrology of freeform shaped parts, *CIRP Ann. - Manuf. Technol.* 56 (2007) 810–835, <https://doi.org/10.1016/j.cirp.2007.10.008>.
- [4] M.G. Guerra, F. Lavecchia, G. Maggipinto, L.M. Galantucci, G.A. Longo, Measuring techniques suitable for verification and repairing of industrial components: a comparison among optical systems, *CIRP J. Manuf. Sci. Technol.* 27 (2019) 114–123, <https://doi.org/10.1016/j.cirp.2019.09.003>.
- [5] G. He, Y. Sang, K. Pang, G. Sun, An improved adaptive sampling strategy for freeform surface inspection on CMM, *Int. J. Adv. Manuf. Technol.* 96 (2018) 1521–1535, <https://doi.org/10.1007/s00170-018-1612-y>.
- [6] M. Aliakbari, M. Mahboubkhah, An adaptive computer-aided path planning to eliminate errors of contact probes on free-form surfaces using a 4-DOF parallel robot CMM and a turn-table, *Meas. J. Int. Meas. Confed.* 166 (2020), 108216, <https://doi.org/10.1016/j.measurement.2020.108216>.
- [7] M. Ren, L. Kong, L. Sun, C. Cheung, A curve network sampling strategy for measurement of freeform surfaces on coordinate measuring machines, *IEEE Trans. Instrum. Meas.* 66 (2017) 3032–3043, <https://doi.org/10.1109/TIM.2017.2717283>.
- [8] L. Schild, F. Sasse, J.-P. Kaiser, G. Lanza, Assessing the optical configuration of a structured light scanner in metrological use, *Meas. Sci. Technol.* 33 (2022), 085018, <https://doi.org/10.1088/1361-6501/ac6e2f>.

- [9] M.R. Dury, S.D. Woodward, S.B. Brown, M.B. McCarthy, Characterising 3D optical scanner measurement performance for precision engineering, *Proc. - ASPE 2016 Annu. Meet.* (2016) 167–172.
- [10] S. Catalucci, N. Senin, D. Sims-Waterhouse, S. Ziegelmeier, S. Piano, R. Leach, Measurement of complex freeform additively manufactured parts by structured light and photogrammetry, *Meas. J. Int. Meas. Confed.* 164 (2020), 108081, <https://doi.org/10.1016/j.measurement.2020.108081>.
- [11] E. Cuesta, S. Giganto, B.J. Alvarez, J. Barreiro, S. Martínez-Pellitero, V. Meana, Laser line scanner aptitude for the measurement of selective laser melting parts, *Opt. Lasers Eng.* 138 (2021), 106406, <https://doi.org/10.1016/j.optlaseng.2020.106406>.
- [12] M.G. Guerra, L. De Chiffre, F. Lavecchia, L.M. Galantucci, Use of miniature step gauges to assess the performance of 3D optical scanners and to evaluate the accuracy of a novel additive manufacture process, *Sensors (Switzerland)*. 20 (2020), <https://doi.org/10.3390/s20030738>.
- [13] S. Lou, S.B. Brown, W. Sun, W. Zeng, X. Jiang, P.J. Scott, An investigation of the mechanical filtering effect of tactile CMM in the measurement of additively manufactured parts, *Meas. J. Int. Meas. Confed.* 144 (2019) 173–182, <https://doi.org/10.1016/j.measurement.2019.04.066>.
- [14] F. Cabanettes, A. Joubert, G. Chardon, V. Dumas, J. Rech, C. Grosjean, Z. Dimkovski, Topography of as built surfaces generated in metal additive manufacturing: a multi scale analysis from form to roughness, *Precis. Eng.* 52 (2018) 249–265, <https://doi.org/10.1016/j.precisioneng.2018.01.002>.
- [15] M. Heinel, S. Greiner, K. Wudy, C. Pobel, M. Rasch, F. Huber, T. Papke, M. Merklein, M. Schmidt, C. Körner, D. Drummer, T. Hausotte, Measuring procedures for surface evaluation of additively manufactured powder bed-based polymer and metal parts, *Meas. Sci. Technol.* 31 (2020), 095202, <https://doi.org/10.1088/1361-6501/ab89e2>.
- [16] J.C. Fox, F. Kim, Z. Reese, C. Evans, Complementary use of optical metrology and x-ray computed tomography for surface finish and defect detection in laser powder bed fusion additive manufacturing, *Proc. - 2018 ASPE Euspen Summer Top. Meet. Adv. Precis. Addit. Manuf.* (2018) 195–200.
- [17] A. Townsend, N. Senin, L. Blunt, R.K. Leach, J.S. Taylor, Surface texture metrology for metal additive manufacturing: a review, *Precis. Eng.* 46 (2016) 34–47, <https://doi.org/10.1016/j.precisioneng.2016.06.001>.
- [18] B. Boeckmans, Y. Tan, F. Welkenhuyzen, Y.S. Guo, W. Dewulf, J.P. Kruth, Roughness offset differences between contact and non-contact measurements, *Proc. 15th Int. Conf. Eur. Soc. Precis. Eng. Nanotechnology, EUSPEN (2015, 2015)*, 189–190.
- [19] L. Schild, A. Kraemer, D. Reiling, H. Wu, G. Lanza, Influence of surface roughness on measurement uncertainty in Computed Tomography, in: *8th Conf. Ind. Comput. Tomogr. Wels, Austria (ICT 2018) Influ.*, 2018: pp. 499–502. <https://doi.org/10.1016/j.cirp.2017.04.067>.
- [20] A.H. Novak, B. Runje, Influence of object surface roughness in CT dimensional measurements More, in: *7th Conf. Ind. Comput. Tomogr. Leuven, Belgium (ICT 2017) Influ.*, 2017: pp. 199–204.
- [21] V. Aloisi, S. Carmignato, Influence of surface roughness on X-ray computed tomography dimensional measurements of additive manufactured parts, *Case Stud. Nondestruct. Test. Eval.* 6 (2016) 104–110, <https://doi.org/10.1016/j.cnsdt.2016.05.005>.
- [22] V.M. Rivas Santos, A. Thompson, D. Sims-Waterhouse, I. Maskery, P. Woolliams, R. Leach, Design and characterisation of an additive manufacturing benchmarking artefact following a design-for-metrology approach, *Addit. Manuf.* 32 (2020), 100964, <https://doi.org/10.1016/j.addma.2019.100964>.
- [23] M.G. Guerra, C. Volpone, L.M. Galantucci, G. Percoco, Photogrammetric measurements of 3D printed microfluidic devices, *Addit. Manuf.* 21 (2018), <https://doi.org/10.1016/j.addma.2018.02.013>.
- [24] H.S. Abdul-Rahman, S. Lou, W. Zeng, X. Jiang, P.J. Scott, Freeform texture representation and characterisation based on triangular mesh projection techniques, *Measurement*. 92 (2016) 172–182, <https://doi.org/10.1016/j.measurement.2016.06.005>.
- [25] L. Pagani, Q. Qi, X. Jiang, P.J. Scott, Towards a new definition of areal surface texture parameters on freeform surface, *Meas. J. Int. Meas. Confed.* 109 (2017) 281–291, <https://doi.org/10.1016/j.measurement.2017.05.028>.
- [26] L. Pagani, A. Townsend, W. Zeng, S. Lou, L. Blunt, X.Q. Jiang, P.J. Scott, Towards a new definition of areal surface texture parameters on freeform surface: Re-entrant features and functional parameters, *Meas. J. Int. Meas. Confed.* 141 (2019) 442–459, <https://doi.org/10.1016/j.measurement.2019.04.027>.
- [27] Y. Qie, L. Qiao, N. Anwer, Enhanced invariance class partitioning using discrete curvatures and conformal geometry, *CAD Comput. Aided Des.* 133 (2021), 102985, <https://doi.org/10.1016/j.cad.2020.102985>.
- [28] M.B. McCarthy, S.B. Brown, A. Evenden, A.D. Robinson, NPL freeform artefact for verification of non-contact measuring systems, *Soc. PhotoOptical.* 7864 (2011) 78640K-78640K-13. <https://doi.org/10.1117/12.876705>.
- [29] M.G. Guerra, F. Lavecchia, L.M. Galantucci, Artefacts Used for Testing 3D Optical-Based Scanners, in: *Lect. Notes Mech. Eng.*, 2020: pp. 173–189. https://doi.org/10.1007/978-3-030-46212-3_12.
- [30] M.G. Guerra, L.M. Galantucci, F. Lavecchia, L. De Chiffre, Reconstruction of small components using photogrammetry: a quantitative analysis of the depth of field influence using a miniature step gauge, *Metro. Meas. Syst.* 28 (2021), <https://doi.org/10.24425/mms.2021.136610>.
- [31] GOM Zeiss, GOM Software: Powerful stand-alone metrology solution and recognized industry standard, (2022). <https://www.zeiss.it/metrologia/innovation-magazine/2021/gom-suite.html> (accessed July 12, 2022).
- [32] H. Villarraga-Gómez, L. Körner, R. Leach, S.T. Smith, Amplitude-wavelength maps for X-ray computed tomography systems, *Precis. Eng.* 64 (2020) 228–242, <https://doi.org/10.1016/j.precisioneng.2020.03.005>.
- [33] H. Villarraga-Gómez, L. Körner, R. Leach, S.T. Smith, Representing the specification of industrial x-ray computed tomography with amplitude-wavelength space, *Proc. - 33rd ASPE Annu. Meet.* (2018) 127–135.